Synsint Research Group

Available online at www.synsint.com

Synthesis and Sintering

**ISSN** 2564-0186 (Print), **ISSN** 2564-0194 (Online)

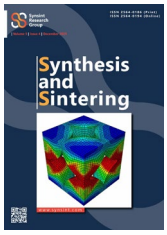


*Research article*

# Simulation of friction stir welding in butt welds of grade 5 titanium alloy and measurement of heat distribution

**Iman Mohammadi** [a,*], **Bahman Mirzakhani** [b]

[a] *Department of Materials Science and Engineering, Faculty of Engineering, Arak University, Arak, 38156-8-8349, Iran*
[b] *Department of Materials Science and Engineering, Faculty of Mechanical Engineering, Shahid Rajaee Teacher Training University, Tehran, Iran*

A B S T R A C T

Residual stresses are generally referred to as stresses that exist in parts without applying external force and loading, and all of the components of these stresses have reached equilibrium with each other in different directions in the part. One of the major problems in welding is the creation of residual stress and distortion due to local heating. As a result of intense heat concentration in the welding area, the areas near the welding experience several thermal cycles. These thermal cycles cause non-uniform heating and cooling of the material and, as a result, create heterogeneous deformations and residual stresses in the part. Friction stir welding (FSW) is one of the widely used welding methods in various industries, such as aerospace. The measurement of heat distribution in the FSW process is an important challenge. In this welding method, the issue of heat transfer, fluid and dynamic equations resulting from tool movement, as well as the cooling of the part up to the temperature of phase transformation in welded parts, play a significant role in accurately predicting the residual stresses caused during welding. In this research study, the regime of cooling and heating of the material, and as a result, the residual stress magnitude during the FSW process, was simulated by using the equations related to heat transfer and temperature-dependent properties of the material. To do the simulation, ABAQUS software was used, accompanied by the DFLUX subroutine. After validating the simulation results by means of experimental welding and tests, the effect of temperature changes on the creation of residual stress resulting from heating and cooling cycles during welding was examined.


KEYWORDS

Friction stir welding (FSW)
Simulation
Residual stress
Thermal history

OPEN ACCESS

## 1. Introduction

Friction stir welding is considered the most significant advancement in metal joining in recent decades. In addition, due to its energy efficiency, environmental compatibility, and adaptability, it is considered a "green" technology. Friction stir welding was initially employed for aluminum alloys and is primarily used in the industry to join various aluminum alloys under casting, rolling, or extrusion conditions [1, 2]. However, similar and dissimilar joining of magnesium alloys, titanium, copper, steel, plastics, and metal matrix composites (MMCs) has also been accomplished through this method [1, 2]. This joining method has applications in various industries, including shipbuilding and maritime, aerospace, rail, automotive, and electronics [1]. Friction stir welding, in its solid-state form, offers advantages over fusion-based joining processes, such as preventing defects associated with melting and solidification, like solidification cracks, reducing distortion resulting from welding, the ability to join many "non-weldable" alloys, and the absence of the need for edge preparation. Like any heat-based manufacturing operation or plastic deformation process, measuring residual stresses resulting from friction

* Corresponding author. *E-mail address:* imohammadi@msa.ir (I. Mohammadi)
Received 22 July 2025; Received in revised form 24 December 2025; Accepted 24 December 2025.

https://doi.org/10.53063/synsint.2025.54297

stir welding is of particular importance. In general, three factors—thermal changes, phase transformations, and mechanical operations—have an impact on the formation of residual stresses [3]. As a result, the microstructure of the weld nugget region experiences various thermomechanical histories and is not uniform. Despite the localized microstructural heterogeneity, one of the notable advantages of this welding method is the fully recrystallized, well-aligned, and fine-grained microstructure formed in the weld nugget through severe plastic deformation at elevated temperatures [4–7]. Titanium alloys have attracted attention in the medical and aerospace industries in recent decades due to their high strength, low elastic modulus, excellent corrosion resistance, and biocompatibility [8]. Titanium alloys are known to present significant challenges during welding due to their high reactivity with atmospheric gases at elevated temperatures, which can lead to microstructural degradation and deterioration of mechanical and functional properties in the welded joint. Solid-state welding techniques are increasingly preferred over fusion welding methods for titanium alloys due to the inherent challenges associated with melting-based processes. Friction stir welding of titanium alloys, especially α and near-α alloys, often faces challenges arising from tool limitations and the thickness of alloy sheets.

A detailed review of the tool dimensions and process conditions for friction stir welding of titanium alloys can be found in the study conducted by Rai and his colleagues [9]. The study conducted by Ji and Li [10] on friction stir lap joint welding of Ti-6Al-4V has indicated that the higher temperature resulting from higher rotation speeds leads to the formation of void defects in the weld. Li et al. [11], in their study on Ti-6Al-4V sheet samples with a thickness of 2 mm, aimed to achieve optimal welding parameters. They classified the rotation speed and traverse speed of the tool to avoid exceeding the temperature from the β-phase solidification temperature.

For titanium alloys with α or near-α phases, the higher coefficient of thermal expansion of the α phase, lower thermal conductivity, and higher heat capacity of titanium make the selection of tool materials challenging for titanium alloys with temperatures above the transus β. β alloys or α + β alloys are more tolerant of the equilibrium temperature of β transus during friction stir welding, depending on the welding parameters and heat distribution along the FSW process. The microstructure's spatial and temporal evolution is driven by temperature and phase transformation in titanium alloys However, measuring the temperature during friction stir welding is not straightforward due to the intense plastic deformation involved in the process. Edwards and Ramulu [12] attempted to measure temperature distribution by placing thermocouples either outside or in the weld region. Their experimental measurements were conducted to determine the maximum temperature during the friction stir welding process of Ti-6Al-4V alloy as a function of process conditions, such as tool rotation speed and traverse speed. It was determined that the tool rotation speed predominantly influences the maximum temperature, while the traverse speed of the tool controls the time exposed to the maximum temperature. A low rotation speed leads to a maximum temperature near or below the β transus temperature of the material (around 1000 °C), while welding at a high rotation speed results in a higher maximum temperature exceeding 1200 °C. It is evident that in friction stir welding of titanium alloys, residual stresses in the weld structure, considering the yield strength of the welded alloy, have a significant ratio and can be a concern for the application of such welds [12]. Edwards and Ramulu [12] investigated the effect of stress-relief heat treatment on reducing residual stresses, measuring residual stresses in friction stir welds of Ti-6Al-4V alloy with lap joint thicknesses ranging from 3 to 12 millimeters. It was found that there are residual tensile stresses along the welding direction and compressive stresses perpendicular to the weld in the post-welding or post-stress-relief heat treatment conditions. Numerous process parameters in friction stir welding influence the residual stress state and, consequently, the distortion of the welded plate. Certainly, all these parameters can affect the temperature profile during the friction stir welding process. The thermal history has a profound impact on the generation of residual stresses, and any alteration in it can affect both thermal stresses and, consequently, residual stresses. Understanding the origin of residual stresses in the welded components is of paramount importance and is key to reducing residual stresses in welds and, consequently, distortions. In this study, the friction stir welding process has been simulated using the Abaqus software. Numerical simulation using the finite element method, through coupled thermal-mechanical numerical analysis, was performed to predict the induced residual stresses during friction stir welding. In the first phase of the simulation, the temperature profile of the workpiece resulting from the tool movement was obtained. In the second stage, to validate the simulation, a sample of titanium alloy was welded, and the temperature was measured at two points (in the temperature-affected zone and along the weld line or weld nugget). Continuing with the validation of simulation results, a Ti-6Al-4V sheet with a thickness of 2 mm underwent friction stir welding.

## 2. Materials and methods

### *2.1. Simulation and numerical analysis*

In this study, numerical simulation of the process was conducted using ABAQUS software. For this purpose, uncoupled heat transfer analysis was employed. To perform the heat transfer analysis, Subroutine Dflux was utilized, taking into account the effects of friction and large plastic deformation. It's worth noting that in this analysis, the tool itself was not simulated; instead, its effects on the workpiece were modeled. The elements used in the simulation were of the Lagrangian type.

### *2.2. Modeling*

In modeling the process, initially, a three-dimensional deformable and solid part with dimensions of 2×100×150 mm was created. The actual specimen consisted of two pieces with dimensions of 2×50×150 mm. In the modeling process, the created specimen was modeled twice the width, and then the real state was simulated using the Partition technique. Considering that the effect of tool movement during the process is being simulated, the tool itself was not modeled. The dimensions of the tool are shown in Fig. 1, and the place of impact of the tool on the workpiece was partitioned in the form of a strip with a width of 12 mm (equal to the diameter of the shoulder of the tool).

The dimensions of the tool are according to Table 1.

Indeed, considering that friction stir welding is a high-temperature process involving large plastic deformations, the thermal properties of the material should be defined as temperature-dependent. The material properties for the mentioned alloy are provided in Tables 2 and 3. In this study, the density of the alloy is considered constant and equal to 4420 kg/m$^3$ [13].

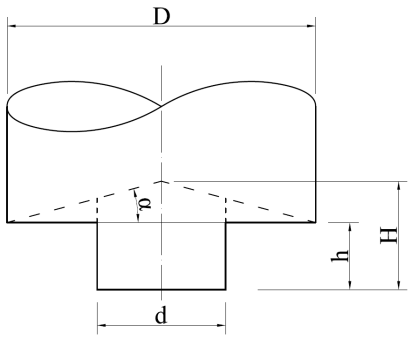


**Fig. 1.** Visualization of the tool.

### *2.3. Analysis steps*

The performed analysis involved two steps of thermal and mechanical analysis. The results obtained from the thermal analysis, including the thermal history of the workpiece during the welding process and subsequent cooling to ambient temperature, were assumed as input for the mechanical analysis. Consequently, residual stresses were calculated based on this thermal history. The welding step of the heat transfer and transient type was created. Due to the dependence of this step on time, the time period in this step was calculated using welding parameters and introduced to the software. To control the temperature at values below the β transient temperature, welding parameters were considered according to Table 3 [13]. The welding time was considered to be 280 s, and the welding path length was set to 140 mm.

In this stage, the minimum increment size was set to $1\times10^{-10}$, the maximum increment size was set to 0.001, and the maximum allowable change in temperature per increment was introduced to the software as 100 °C. Then, another thermal step was created in which the workpiece temperature after completing the welding step was cooled down to ambient temperature. For this purpose, the cooling step duration was set to a large value, specifically 20000 s (more than 5 h), to ensure the workpiece temperature reached ambient temperature. After defining the two main steps of the thermal problem solution, the field output for this part of the problem was also defined as nodal temperature (NT) of the workpiece.

### *2.4. Boundary condition*

One of the major sources of residual stress in welded components is heat loss. Heat dissipation occurs through two mechanisms: radiation and convection. In order to determine the contribution of each of these two terms and the amount of cooling in the workpiece, heat dissipation from the vicinity of the welded area has been considered as radiation at high temperatures, while with decreasing temperature, convection plays the primary role in heat dissipation [13]. A temperature-dependent heat transfer coefficient (Eq. 1) has been proposed that includes both radiation and convection [14].

$$h = 0.0668T \quad (W/m^2) \quad 0<T<500\ °C \tag{1}$$

$$h = 0.231T - 82.1 \quad (W/m^2) \quad 0<T<500\ °C \tag{2}$$

Boundary conditions were applied to all surfaces of the workpiece, and the ambient temperature was considered to be 25 °C. In the mechanical analysis, the lateral faces of the workpiece were constrained, meaning the degrees of freedom, i.e., displacement along the three axes, were restricted.

### *2.5. Loading*

In this simulation, the heat flux (heat input per unit volume per unit time) to the workpiece was applied along the welding path by a moving heat source. The moving heat source has geometric and motion specifications. To determine the thermal fields, subroutine DFLUX was used. To determine the heat flux in welding, the Goldak model was used [15]. In this model, the relationships related to heat flux are defined as two semi-ellipsoidal (Fig. 2) models in the front half and the back half as follows (Eq. 3 and 4).

Heat flux in the back half:

$$q_r(x,y,z) = \frac{6\sqrt{3}f_r Q_t}{abc_r\pi\sqrt{\pi}} e^{(-3x^2/a^2)} e^{(-3y^2/b^2)} e^{(-3z^2/c_r^2)} \tag{3}$$

Heat flux in the front half:

$$q_f(x,y,z) = \frac{6\sqrt{3}f_f Q_t}{abc_f\pi\sqrt{\pi}} e^{(-3x^2/a^2)} e^{(-3y^2/b^2)} e^{(-3z^2/c_f^2)} \tag{4}$$

**Table 1.** Dimensional specifications of the tool.

| | |
|---|---|
| **Shoulder diameter (D), mm** | 0.016 |
| **Pin diameter (d), mm** | 0.052 |
| **Pin height considering sloping shoulder (H), mm** | 0.0018 |
| **Pin height considering flat shoulder (h), mm** | 0.0018 |
| **Angle of inclination of the shoulder (α), °** | 0 |

**Table 2.** Temperature-dependent thermal properties of Ti-6Al-4V alloy [13].

| Temperature (°C) | Thermal conductivity (W/m.°C) | Heat capacity (J/kg.°C) |
|---|---|---|
| 20 | 7 | 546 |
| 205 | 8.75 | 584 |
| 500 | 12.6 | 651 |
| 995 | 22.7 | 753 |
| 1100 | 19.3 | 641 |
| 1200 | 214 | 660 |
| 1600 | 25.8 | 732 |
| 1650 | 83.5 | 831 |
| 2000 | 83.5 | 831 |

**Table 3.** Welding parameters.

| Welding speed | Rotational speed |
|---|---|
| 0.0005 m/s (30 mm/min) | 83.77 rad/s (~800 rpm) |

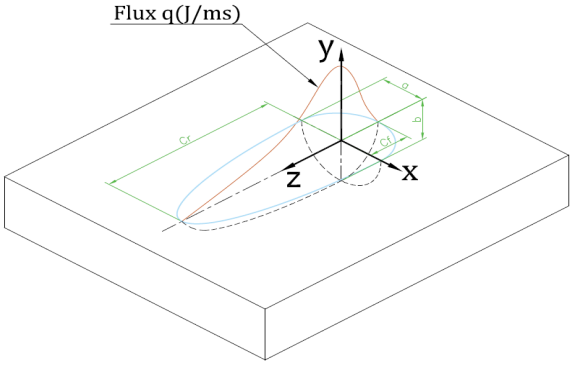


**Fig. 2.** Schematic of the Goldak's two semi-ellipsoidal heat source model [15].

The constants related to the Goldak relation were defined in Table 4. Thus, a= 0.009 m, b=0.002 m, $c_f$ = 0.009 m, $c_r$ = 0.018 m, $f_f$ =1, and $f_r$ =1.

In relation to heat flux, $Q_t$ is the heat caused by welding, and the rest of the constants are related to the welding parameters. To calculate the heat flux according to the above equations, the total heat generated, $Q_t$, resulting from the FSW process needs to be determined. The heat generated during the two main tribological processes occurs at the contact interface between the tool and the welded products, involving both pure sliding-adhesion and pure sticking-deformation. It has been assumed that the conditions of the pure sliding condition fully adhere to Coulomb's law. It is also assumed that the pressure between the tool and the weld piece -p- and the friction coefficient -μ- are constant values or independent of other variables [16].

Heat in FSW originates from six different sources:

- Heat generated at the pin tip surface, caused by plastic deformation:

$$Q_{pt}^{deformation} = \frac{2}{3}\pi.\omega.\tau.\frac{1}{8}\left[d^3 - d_0^3\right] \quad (5)$$

where, ω is the tool angular velocity during welding, τ is the shear stress, and $d_0$ is the initial hole diameter formed at the tool plunge location ($d_0$<d).

**Table 4.** The constants related to the Goldak model [16].

| Parameter | In FSW | Definition |
|---|---|---|
| a | Little more than shoulder diameter | Half of the heat flux area |
| b | Thickness of plate | Depth of heat penetration due to heat flux - greater than the depth of weld penetration |
| $c_f$ | Equal to a | Front length of heat-affected zone (HAZ) |
| $c_r$ | Equals to 2a | Rear length of HAZ |
| $f_f$ | 1 | Fraction of total heat applied to the front portion of Goldak's model |
| $f_r$ | 1 | Fraction of total heat applied to the rear portion of Goldak's model |

- Heat generated at the pin tip surface, caused by friction:

$$Q_{pt}^{friction} = \frac{2}{3}\pi.\mu.p.\omega.\frac{1}{8}\left[d^3 - d_0^3\right] \quad (6)$$

where, μ and p are the friction coefficient and pressure between the tool and the weld piece, respectively.

- Heat generated at the pin side surface, caused by plastic deformation:

$$Q_{ps}^{diformation} = 2\pi.\tau.\omega.\frac{1}{8}(\frac{d}{2})^2.H \quad (7)$$

- Heat generated at the pin side surface, caused by friction:

$$Q_{ps}^{friction} = \frac{2}{3}\pi.\mu.p.\omega.(\frac{d}{2})^2.H \quad (8)$$

- Heat generated at the shoulder tip surface, caused by plastic deformation:

$$Q_{st}^{diformation} = \frac{2}{3}\pi.\tau.\omega.\frac{1}{8}\left[D^3 - d^3\right].(1+\tan\alpha) \quad (9)$$

- Heat generated at the shoulder tip surface, caused by plastic friction:

$$Q_{st}^{friction} = \frac{2}{3}\pi.\mu.p.\omega.\frac{1}{8}\left[D^3 - d^3\right].(1+\tan\alpha) \quad (10)$$

The total heat generated by the process is the sum of the above-mentioned heats, where ultimately, a portion of it is due to friction in different sections, and a portion is due to the severe plastic deformation in the workpiece caused by the movement of the tool. To determine the contribution of friction and plastic deformation to the total heat, the parameter δ is defined. This parameter is expressed as a function of the ratio of the velocity of contact points at the welding location ($V_{cp}$) to the linear velocity resulting from the angular speed of the tool ($V_\omega$), $\delta = V_{cp}/V_\omega$. Based on this, the total heat will be:

$$Q_{total} = (1-\delta)Q_{friction} + \delta Q_{deformation}\ [16] \quad (11)$$

After substitution and simplification, Eq. 12 is obtained.

$$Q_{total} = \frac{1}{12}\pi.\omega\left[(1-\delta)\mu.p + \delta.\tau\right]\left[\left[D^3 - d^3\right].(1+\tan\alpha) + \left[d^3 - d_0^3\right] + 6d^2H\right] \quad (12)$$

which, by ignoring the heat from the side surfaces and simplifying assumptions (α=0, $d_0$=d, $Q_{pt}$=0, and $Q_{ps}$=0), becomes the following equation.

$$Q_{total} = \frac{1}{12}\pi.\omega\left[(1-\delta)\mu.p + \delta.\tau\right]\left[D^3 - d^3\right] \quad (13)$$

In the FSW process, it is considered that half of the heat is due to friction, and the other half is due to plastic deformation. Therefore, δ=0.5 is taken into account [16]. Therefore, the required $Q_t$ was calculated in Goldak relations. According to the parameters related to the present study, $Q_t$ = 6640 J was obtained. Now referring back to Goldak's front and back semi-elliptical relations, the term $6\sqrt{3}Q/(ab\pi\sqrt{\pi})$, which is common in both relations, was assumed to be equal to $Q_0$. In this way, the heat flux location equation, after dwell time (T>T1), was applied in two situations: z≤zc (back semi-ellipse) and z>zc (front semi-ellipse) [16].

It should be noted that zc is the coordinate of the welding position along the z axis and at time t, according to the linear speed of welding v = 0.0005 m/s. Eq. 14 shows the coordinates of the place where the flux is applied as a function of time.

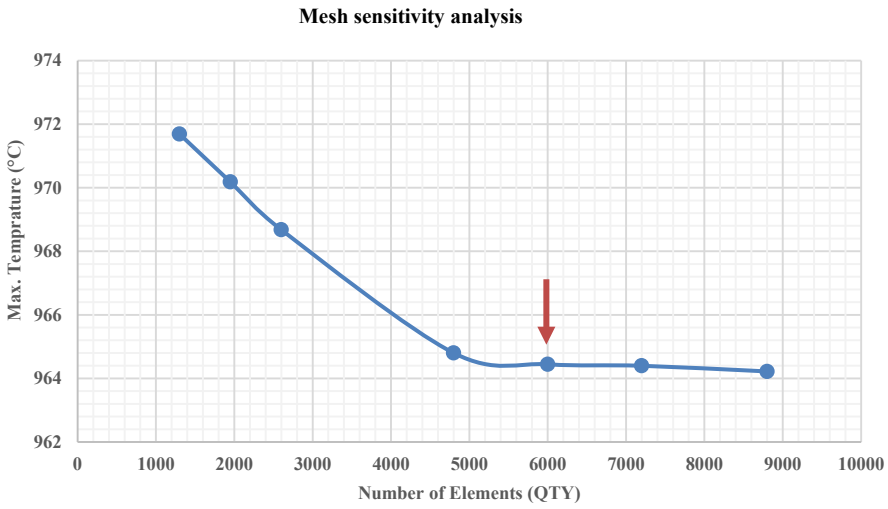


**Fig. 3.** Mesh sensitivity analysis: optimal number of elements.

$$v = \frac{z}{t} \Rightarrow z = v.t \Rightarrow z = v(T + tt_0) \quad tt_0\text{: dwell time} \tag{14}$$

To apply the heat source along the welding path for thermal analysis, the option "body heat flux" was used.

### *2.6. Meshing*

For meshing the model, the "Bias" meshing technique was utilized. In this process, the $DC_3D_8$ mesh type (an 8-node linear heat transfer brick) was employed, which has a temperature degree of freedom (coupled temperature displacement). In the regions adjacent to the weld seam, a finer mesh size was chosen to ensure a more accurate analysis. In the regions adjacent to the weld seam, a finer mesh size was chosen to ensure a more accurate analysis (Fig. 3). The sensitivity analysis of mesh refinement was conducted by examining the variable "maximum temperature".

The goal was to achieve an optimal number of elements. By conducting this analysis and plotting the maximum temperature versus the number of elements, the optimal number of elements was determined to be 6000 with 12382 nodes. The mesh of the model is shown in Fig. 4.

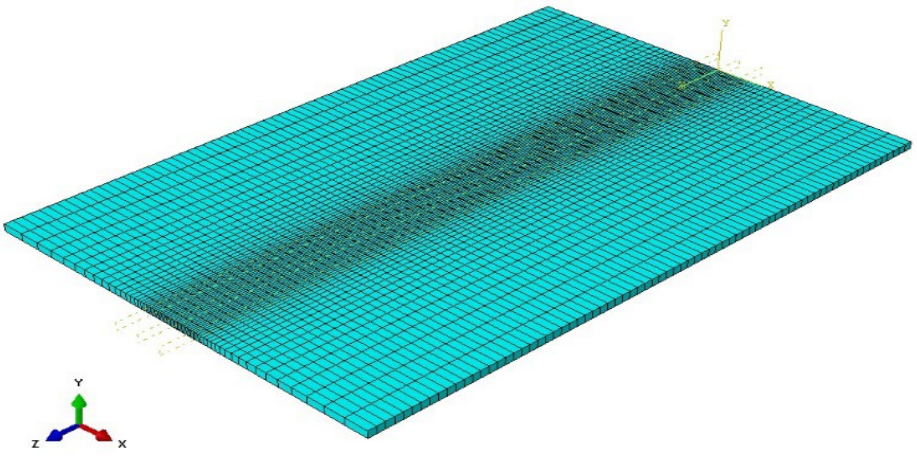


**Fig. 4.** Mesh of the model.

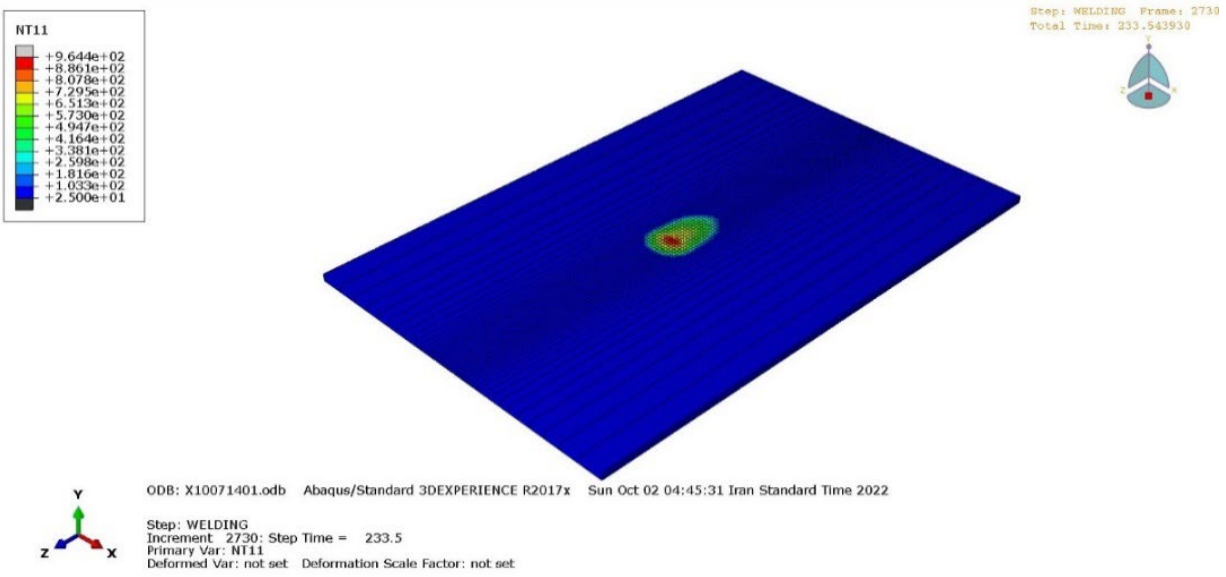


**Fig. 5.** Temperature profile of the part when the tool passes through the center point of the welding line.

### *2.7. Extracting the results*

The temperature history of a point on HAZ and the center weld line point, which is part of the welding path, has been extracted. The temperature profile of this point during welding is shown in Fig. 5.

### *2.8. Experimental tests*

#### *2.8.1. Base metal and determine its basic characteristics*

In order to measure the heat distribution during the friction-stir welding process, a sheet of Ti-6Al-4V alloy with dimensions of 2×100×150 mm was prepared. In the middle of the sheet width, a line was embedded using a punch, and the location of the tool plunge was created as a hole equivalent to the pin diameter (4 mm) [11].

The chemical analysis of the mentioned components was determined by the spectrometric method according to the ASTM E-2998-2016 standard, reported in weight percentage using the Oxford instrument. The results are presented in Table 5.

In addition, a sample of the base metal was prepared according to the ASTM E3-2017 standard for metallographic sample preparation. The metallographic analysis was performed following the ASTM E407-2015 standard in an acidic solution consisting of 10 ml HF + 5 ml $HNO_3$ + 85 ml $H_2O$.

Then, metallographic images were prepared in accordance with the ASTM E883-2017 standard with two magnifications, 100X and 500X. As shown in Fig. 7, the structure consists of scattered β-phase in the α-phase matrix.

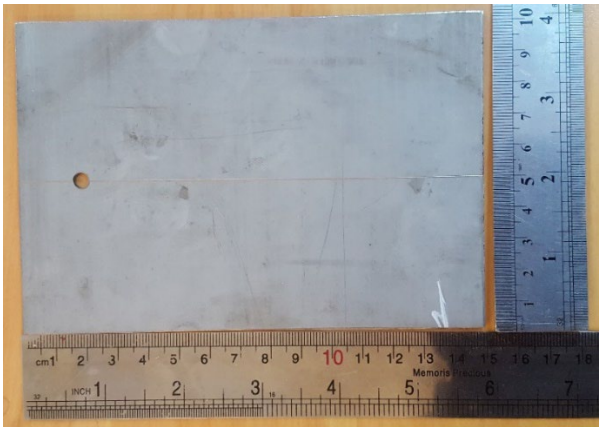

**Fig. 6.** Workpiece geometry and dimensions.


**Fig. 7.** Metallographic image of base metal. The bright matrix is α-phase, and the dark region is β-phase.

**Table 5.** Chemical analysis of base metal (Ti-6Al-4V).

| Element | Weight percentage (wt%) |
|---|---|
| Ti | Base |
| Al | 6.35 |
| V | 3.86 |
| Cr | <0.005 |
| Cu | <0.005 |
| Fe | 0.14 |
| Mn | <0.005 |
| Mo | <0.01 |
| Nb | <0.005 |
| Ni | 0.007 |
| Si | 0.02 |
| Zr | 0.02 |
| Pd | <0.01 |
| Ru | <0.01 |
| Sn | <0.02 |

The mechanical properties were obtained through tensile testing on the samples, as described in Table 6. Considering the thickness of the sheet, microhardness testing was performed using the Vickers scale, resulting in an average hardness of 350 Hv10.

### *2.8.2. Tool design*

The material available for the tool is tungsten carbide [9]. According to the optimal dimensions mentioned in the references, the tool was prepared in accordance with Fig. 8 [11].

In order to ensure the strength of the tool during the process, the hardness of the tool was measured. The hardness of the tool was found to be 69.7 HRC in the Rockwell C standard. Then, the workpiece was completely fixed and then welded with a rotational speed of 800 rpm and a tool transverse speed of 30 mm/s. To protect the welding area from oxidation, argon grade 5 shielding gas (purity 99.999%) was used. The temperature of the heat-affected zone (HAZ) and below the weld line was measured using a type K thermocouple. Comparing the measured temperatures with the temperatures calculated by the software is a crucial step to validate the simulation.

**Table 6.** Mechanical properties of base metal.

| | | |
|---|---|---|
| **Longation A (%)** | | 4 |
| **Yield strength, $R_m$ (MPa)** | | 1197 |
| **Yield strength, $R_t$ (MPa)** | | 1167 |
| **Dimension of samples** | **Gauge length** | $L_0$: 50 mm |
| | **Cross section** | $S_0$: 28.42 $mm^2$ |
| | **Width×height** | 13.06 mm×2.06 mm |

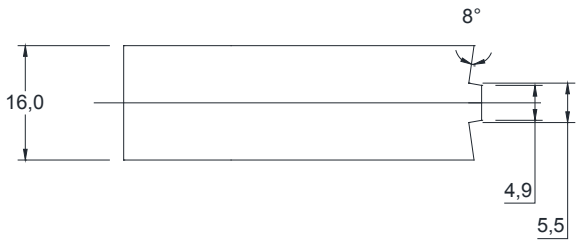


**Fig. 8.** Dimensional characteristics of tool [11].

## 3. Results and discussion

The temperature history at the two points of the center of the weld line and the temperature-affected area was extracted from the simulation results. The temperature history at the two points of the center and HAZ was extracted from the simulation results, which is shown in Fig. 9a & b.

In Fig. 10a & b, the thermal history at the two points of the center and HAZ, which is extracted from the results of the tests, is shown.

By comparing the temperatures calculated from the simulation results and the temperatures measured in the practical tests, the appropriate accuracy of the simulation was proved.

## 4. Conclusions

- The analysis shows a reasonable accuracy with an approximately 80-degree Celsius difference compared to the experimentally obtained maximum temperature.
- The sensitivity of the maximum temperature to the diameter of the tool shoulder was observed. It implies that the diameter of the tool shoulder has an impact on the maximum temperature reached during the process. This sensitivity can be crucial in understanding and optimizing the friction stir welding process.
- In this analysis, efforts were made to control the maximum temperature reached in the weld line, aiming to eliminate its effects on heat distribution at temperatures lower than the phase transformation temperature. It is recommended that in similar research, the effects of phase transformation be taken into account. Understanding and considering phase transformation effects are crucial for a comprehensive analysis of the material behavior during and after the welding process.

## CRediT authorship contribution statement

**Iman Mohammadi:** Data curation, Formal Analysis, Validation, Visualization, Software, Writing – original draft.

**Bahman Mirzakhani**: Conceptualization, Methodology, Project administration, Supervision, Writing – review & editing.

## Data availability

The data underlying this article will be shared on reasonable request to the corresponding author.

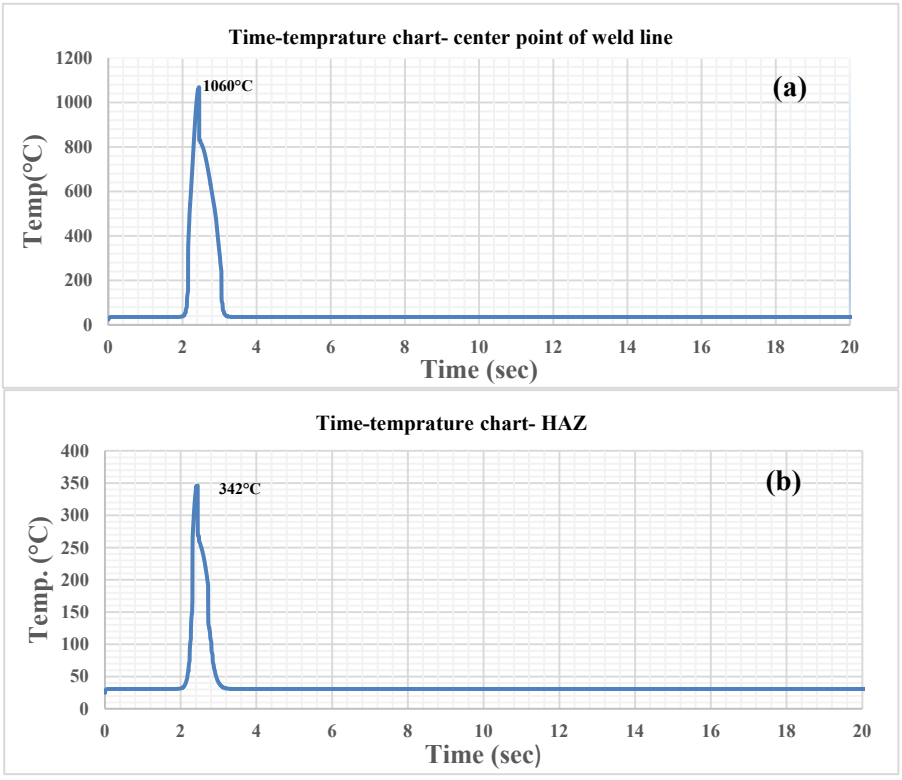


**Fig. 9.** Thermal history obtained from the simulation results in a) central point of weld line and b) HAZ.

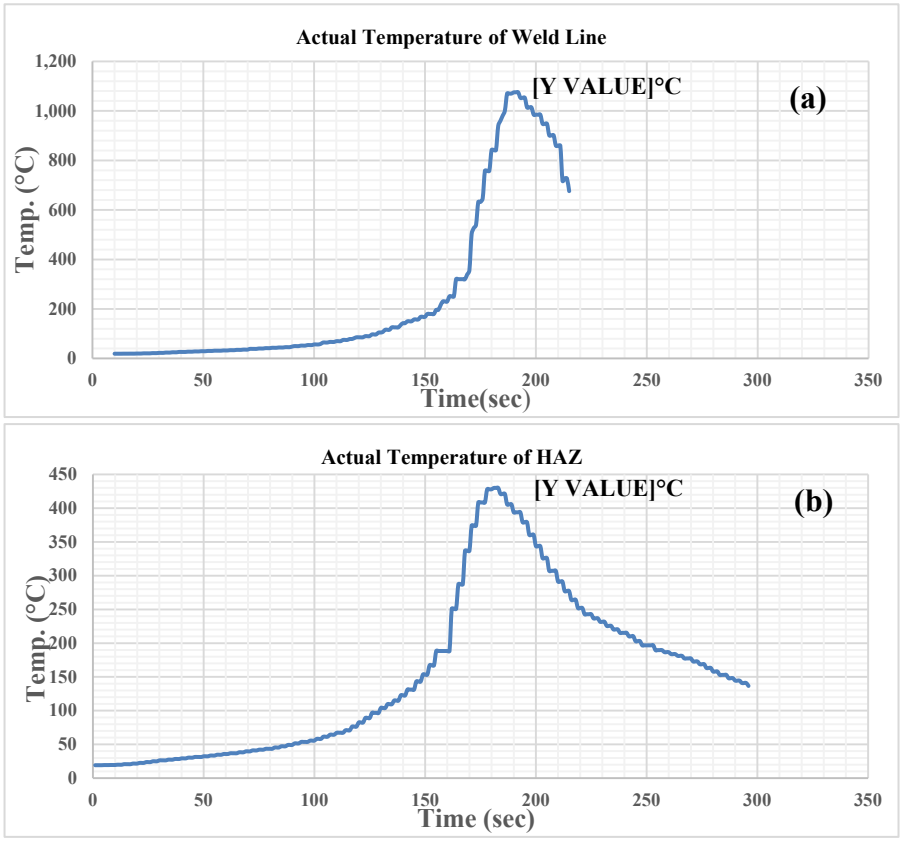


**Fig. 10.** Thermal history obtained from experimental results in a) center point of weld line and b) HAZ.

## Declaration of competing interest

The authors declare no competing interests.

## Funding and acknowledgment

This research received no external funding. The authors would like to thank the Welding Laboratory of Tarbiat Modares University and its supervisor for providing experimental facilities and technical support.

## References

[1] W.M. Thomas, E.D. Nicholas, J.C. Needham, M.G. Murch, P. Templesmith, C.J. Dawes, International Patent Application No. PCT/GB92/02203 and GB Patent Application No. 9125978.8. (1991).
[2] C. Dawes, W. Thomas, TWI Bull. 6 (1995) 124.
[3] B. London, M. Mahoney, B. Bingel, M. Calabrese, D. Waldron, in Proceedings of the Third Int. Symposium on Friction Stir Welding, Kobe, Japan. (2001) 27–28.
[4] C.G. Rhodes, M.W. Mahoney, W.H. Bingel, R.A. Spurling, C.C. Bampton, Effects of friction stir welding on microstructure of 7075 aluminum, Scr. Mater. 36 (1997) 69–75. https://doi.org/10.1016/S1359-6462(96)00344-2.
[5] G. Liu, L.E. Murr, C.S. Niou, J.C. Mc - Clure, F.R. Vega, Microstructural aspects of the friction-stir welding of 6061-T6 aluminum, Scr. Mater. 37 (1997) 355–361. https://doi.org/10.1016/S1359-6462(97)00093-6.
[6] K.V. Jata, S.L. Semiatin, Continuous dynamic recrystallization during friction stir welding of high strength aluminum alloys, Scr. Mater. 43 (2000) 743–749. https://doi.org/10.1016/S1359-6462(00)00480-2.
[7] S. Benavides, Y. Li, L.E. Murr, D. Brown, J.C. McClure, Low-Temperature Friction-stir Welding of 2024 Aluminum, Scr. Mater. 41 (1999) 809–815. https://doi.org/10.1016/S1359-6462(99)00226-2.
[8] X.K. Zhu, Y.J. Chao, Numerical simulation of transient temperature and residual stresses in friction stir welding of 304L stainless steel, J. Mater. Process. Technol. 146 (2004) 263–272. https://doi.org/10.1016/j.jmatprotec.2003.10.025.
[9] R. Rai, A. De, H.K.D.H. Bhadeshia, T. DebRoy, Review: friction stir welding tools, Sci. Technol. Weld. Join. 16 (2011) 325–342. https://doi.org/10.1179/1362171811Y.0000000023.
[10] S. Ji, Z. Li, Reducing the hook defect of friction stir lap welded Ti-6Al-4V alloy by slightly penetrating into the lower sheet, J. Mater. Eng. Perform. 26 (2017) 921–930. https://doi.org/10.1007/s11665-017-2512-2.
[11] J. Li, Y. Shen, W. Hou, Y. Qi, Friction stir welding of Ti-6Al-4V alloy: Friction tool, microstructure, and mechanical properties, J. Manuf. Process. 58 (2020) 344–354. https://doi.org/10.1016/j.jmapro.2020.08.025.
[12] P. Edwards, M. Ramulu, Surface residual stresses in Ti-6Al-4V friction stir welds: pre-and post-thermal stress relief, J. Mater. Eng. Perform. 24 (2015) 3263–3270. https://doi.org/10.1007/s11665-015-1610-2.
[13] X. Lu, X. Lin, M. Chiumenti, M. Cervera, Y. Hu, et al., Residual stress and distortion of rectangular and S-shaped Ti-6Al-4V parts by Directed Energy Deposition: Modelling and experimental calibration, Addit. Manuf. 26 (2019) 166–179. https://doi.org/10.1016/j.addma.2019.02.001.
[14] B. Brickstad, B. Josefson, A parametric study of residual stresses in multi-pass butt-welded stainless steel pipes, Int. J. Press. Vessel. Pip. 75 (1998) 11–25. https://doi.org/10.1016/S0308-0161(97)00117-8.
[15] J. Goldak, A. Chakravarti, M. Bibby, A new finite element model for welding heat sources, Metall. Trans. B. 15 (1984) 299–305. https://doi.org/10.1007/BF02667333.
[16] A.E. Pour Arsanjan, E. Nazari, M. Ajabshiri, B. Medghalchi, Experimental and finite element measurements of heat distribution in oxygen-free friction stir welding of copper, 12th Iran Conference on Manufacturing and Production Engineering, Tehran. (2010) 25.